International Journal of Mechanical, Industrial and Aerospace Sciences
ISSN: 2517-9950
Vol:12, No:5, 2018

An Experimental Study of Downstream Structures on the Flow-Induced Vibrations Energy Harvester Performances

Pakorn Uttayopas, Chawalit Kittichaikarn

***Abstract*—**This paper presents an experimental investigation for the characteristics of an energy harvesting device exploiting flow-induced vibration in a wind tunnel. A stationary bluff body is connected with a downstream tip body via an aluminium cantilever beam. Various lengths of aluminium cantilever beam and different shapes of downstream tip body are considered. The results show that the characteristics of the energy harvester's vibration depend on both the length of the aluminium cantilever beam and the shape of the downstream tip body. The highest ratio between vibration amplitude and bluff body diameter was found to be 1.39 for an energy harvester with a symmetrical triangular tip body and $L/D_1 = 5$ at 9.8 m/s of flow speed (Re = 20077). Using this configuration, the electrical energy was extracted with a polyvinylidene fluoride (PVDF) piezoelectric beam with different load resistances, of which the optimal value could be found on each Reynolds number. The highest power output was found to be 3.19 μW, at 9.8 m/s of flow speed (Re = 20077) and 27 MΩ of load resistance.

***Keywords*—**Downstream structures, energy harvesting, flow-induced vibration, piezoelectric material, wind tunnel.

I. Introduction

HARVESTING energy from ambient sources has been the subject of several studies in recent years for operating self-powered devices [1]-[3]. Many researchers have devoted their attention to studying flow-induced vibrations as a sustainable power source, because it can be used in small volumes. One of several methods to convert this wasted mechanical vibration into usable electrical energy is through the use of piezoelectric materials [4]-[7].

When a bluff body is immersed in fluid flow, aero-elastic vibration will occur. In additional, a vortex generated from an upstream bluff body can induce downstream structures to vibrate. Many studies have found that an optimal spacing between the upstream bluff body and downstream structure can cause downstream structures to severely oscillate compared to a single bluff body [8], [9]. However, in term of energy harvesting applications, it can enhance the energy harvester performance [10], [11].

This work presented an experimental optimization and study of piezoelectric-based energy harvester exploiting flow-induced vibration. Based on the concept to enhance downstream energy harvester performance, the energy harvesters were designed to have an aluminium cantilever beam and a tip body behind a fixed cylindrical bluff body. With a suitable length of cantilever beam and a suitable shape of downstream tip body, vortices from upstream bluff body can interact with the downstream structure directly causing high amplitude vibration. Many studied rarely paid attention to an effect of downstream tip body's geometries for oscillation-based energy harvesting application. Hence, the different configurations of downstream tip body and various length of cantilever beam were experimentally investigated in a wind tunnel at Reynolds number between 3000 and 20100 to study energy harvester vibration behavior. The configuration with the largest deformation of cantilever beam is considered as an optimized energy harvester. The PDVF piezoelectric type then attach to the trailing edge of a cantilever beam where the maximum strain can be obtained. Power output was then presented with different load resistances which can be found an optimal value to provide the highest electrical power output. Such a harvester has an advance of simplicity which deserves further developments.

Pakorn Uttayopas is with the Department of Mechanical Engineering, Kasetsart University, Bangkok, Thailand (e-mail: mindgats@gmail.com).
Chawalit Kittichaikarn is with the Department of Mechanical Engineering, Kasetsart University, Bangkok, Thailand (corresponding author, e-mail: fengclk@ku.ac.th).

II. Experiment Setup

The experiments were conducted in a low turbulence wind tunnel with open loop and 300 mm x 300 mm test section (Fig. 1). The flow speed is produced by an axis fan which sucks the air in the end of the tunnel. By varying frequency voltage input of fan motor, the flow speed in this section was varied in the range of 1.55 to 9.8 m/s (3000-20100 Reynolds number).

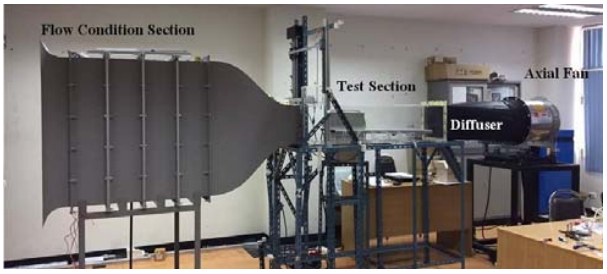

Fig. 1 Low turbulence wind tunnel

Fig. 2 illustrates the designed energy harvester in this study. The energy harvester comprises a stationary aluminium cylindrical bluff body (D_1=32 mm and H=300 mm) affixed to a 3D printed polylactide (PLA) type downstream tip body via

a 0.5 mm thick, 25 mm width and variable length (L) aluminium cantilever beam. The trailing edge was kept free in order to permit vibration only at the cross flow. To optimize the energy harvester's operating conditions, the vibration characteristics of the energy harvester were analyzed from different configurations which consisted of different shapes of tip body: symmetric triangular, cylindrical, and square prisms; and varied lengths of aluminium cantilever beam (L/D_1= 3, 4 and 5). The dimensions of the downstream tip body were all identical, 32 mm in width and 100 mm in height.

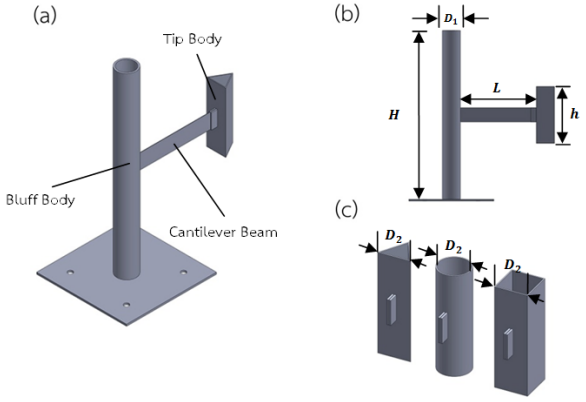

Fig. 2 Illustration of the proposed oscillation-based energy harvesting devices: (a) Isometric view (b) side view (c) illustration of the various tip body configurations, from left to right symmetrical triangular, cylindrical and square prisms

Table I presents properties for each configuration. The structure natural frequency (f_n) can be estimated with (1)

$$f_n = \sqrt{\frac{3EI}{mL^3}} \tag{1}$$

where E is the Young's modulus of aluminium, I is a moment of inertia for each configuration which can be estimated using (2)

$$I = \frac{bd^3}{12} \tag{2}$$

where d is width of aluminium cantilever beam, and b is its thickness. While total mass consists of tip body mass (m_t) and approximately 33/144 of aluminium cantilever beam mass (m_b) as shown in (3)

$$m = \frac{33}{140} m_b + m_t \tag{3}$$

Fig. 3 illustrates the energy harvester installed in the test section of the wind tunnel. The experiment conducted through varied Reynolds number based on upstream bluff body diameter calculated with (4).

TABLE I
ENERGY HARVESTER'S STRUCTURE PROPERTIES

Shape of tip body	Tip Mass, m_t(g)	Width, D_2(mm)	L/D_1	Total Mass, m(g)	Natural frequency, f_n(Hz)
Symmetrical	8.699	32	3	11.2770	11.6987
Triangular			4	11.8793	7.4034
Prism			5	12.4816	5.1680
Cylindrical	8.666	32	3	11.2440	11.7158
Prism			4	11.8463	7.4137
			5	12.4486	5.1749
Square	10.508	32	3	13.0860	10.8600
Prism			4	13.6883	6.8968
			5	14.2906	4.8299

$$\mathrm{Re} = \frac{U_\infty D_1}{\nu} \tag{4}$$

where, ν is the kinematic viscosity of air, while U_∞ is the flow speed varied from 1.55 m/s to 9.8 m/s measuring via a Pitot tube anemometer before the start of the experiments. As a result, Reynolds number has range between 3000 and 20100. A 120 frames-per-second video camera was installed above the test section to record harvester's respond to subjected flow. The recorded videos were then analyzed in image processing program to generated vibration amplitude response as a function of time. The transverse vibration amplitudes (A) were measured from equilibrium base line (Fig. 4) and then summarized into root mean square amplitude (A_{rms}) for each Reynolds number. Applying fast Fourier transformation technique to experimental results resulted in obtaining energy harvester's frequency respond (f_o). The RMS amplitude and frequency response were then presented as non-dimensional value, RMS amplitude ratio (δ) and frequency amplitude ratio (f_{ratio}) calculated using (5) and (6) respectively.

$$\delta = \frac{A_{rms}}{D_1} \tag{5}$$

$$f_{ratio} = \frac{f_o}{f_n} \tag{6}$$

The RMS amplitude ratio and frequency ratio were then compared with the non-dimensional reduced velocity (U_r), which is calculated with (7).

$$U_r = \frac{U_\infty}{f_o D_2} \tag{7}$$

The presented characteristics of energy harvest for each configuration was analyzed and investigated to seek the optimal condition for energy harvesting. The proper configuration was then selected to find electrical energy output in the next step.

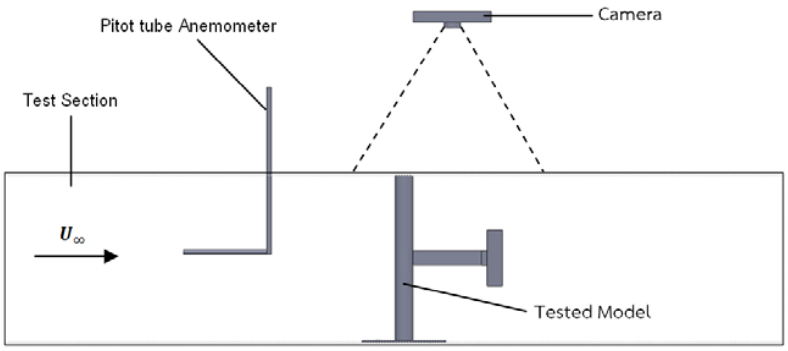

Fig. 3 Schematic diagram of experiment in the wind tunnel

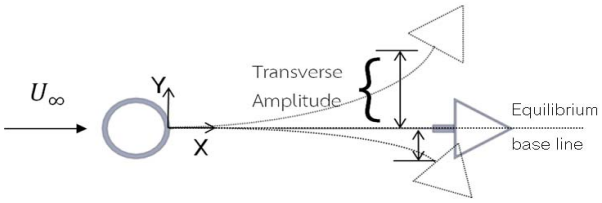

Fig. 4 Top view of energy harvester's encounter of incoming flow

The selected configuration was attached with a piezoelectric beam on one side of the root of aluminium cantilever beam where the maximum strain can be obtained. A PVDF piezoelectric beam (Fig. 5) (LDT1-028K/L w/rivets, Measurement Specialties, Inc., U.S.A) is 41.40 mm in length and 16.26 mm in width and has 1.38 nF of capacitance (C_p). Given the energy harvester in the same range of Reynolds number, an electrical voltage (V) from energy harvester through different load resistances (R) was obtained via a NI USB-6211 data acquisition system in conjunction with LabVIEW at a sampling rate of 1 kHz as shown in Fig. 6. The electrical power output (P) was then presented as a RMS value calculate with (8)

$$P_{rms} = \frac{V_{rms}^2}{R} \tag{8}$$

where V_{rms} is root mean square value of voltage for each Reynold number and R is load resistance ranged from 1 MΩ to 100 MΩ. According to Guyomar et al. [12], the optimal load resistance (R_{opt}) that provides the maximum electric power output can be estimated using (9)

$$R_{opt} = \frac{1}{2\pi f_o C_p} \tag{9}$$

The electrical response of energy harvester in term of power output as a function of load resistance was analyzed and presented to study the influence of load resistance and to seek the maximum power output on the optimal configuration of energy harvester.

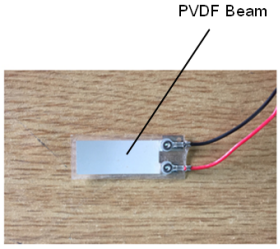

Fig. 5 LDT1-028K/L w/rivets piezoelectric beam

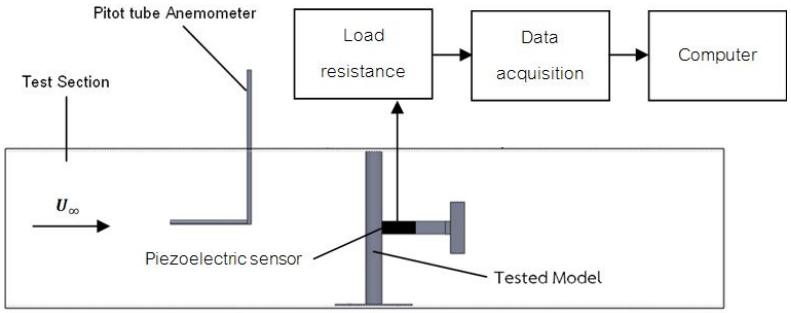

Fig. 6 Schematic diagram of experiment in the wind tunnel for measuring electric voltage

III. Results and Discussion

A. Vibration Amplitude Response

Fig. 7 presents the RMS amplitude ratio of an energy harvester with a symmetric triangular, cylindrical and square prisms downstream tip body as a function of reduced velocity for L/D_1 ratio = 3. Given the rise in flow speed, the RMS amplitude ratios for all configurations have a tendency to increase except for the square prism tip body. The highest

RMS amplitude ratio was found to be 0.39 for the cylindrical prism tip body at approximately 35 of reduced velocity (*Re*=20077).

For the symmetric triangular tip body, there was no response of the RMS amplitude ratio unit as the reduced velocity reached approximately 25 (*Re* = 16389), where it began to respond. Afterward, the RMS amplitude ratio continued to increase dramatically with the increase in flow speed and hit its peak at 0.21 for the highest reduced velocity.

The peak amplitude related to the resonance of the upstream shedding vortex was noted at a reduced velocity between 4 and 7 for the cylindrical tip body. Increasing the reduced velocity further in this region, the RMS amplitude ratio dropped-off and then increased at 12 of reduced velocity. The RMS amplitude ratio continued to rise and reached a peak at 0.39 for 35 of reduced velocity. This value was considered the highest RMS amplitude ratio for L/D_1 ratio = 3.

On the other hand, the square prism tip body seemed to rarely vibrate compared to other shapes of tip body. Even when the flow speed was boosted to its maximum speed, only little buffering response was found.

Typically, when reduced velocity is between 4 and 7, the strong vibration response may be caused by upstream shedding vortices frequency resonant with the structure's natural frequency. However, the energy harvesters with a symmetrical triangular and square prism tip body do not display those types of responses. A strong vibration when increasing the flow speed was noted only for the triangular tip body and no response was found for the square tip body. This might be due to the shape of the downstream tip body. When the separated flow from an upstream bluff body flows over the downstream tip body, the triangular and square prism tip bodies diminish the upstream vortex, while the cylindrical tip body allows an upstream vortex to form.

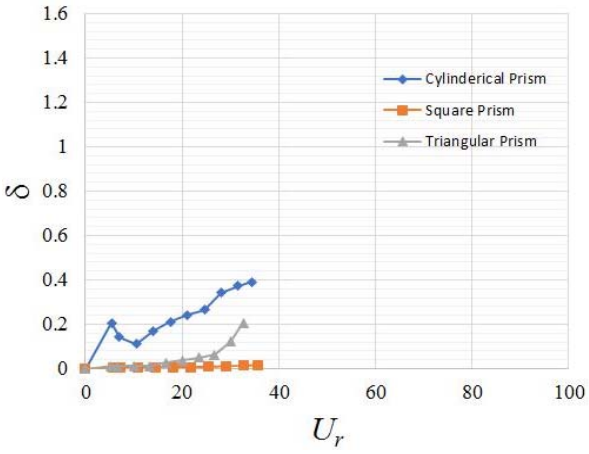

Fig. 7 the RMS amplitude ratio as a function of reduce velocity for $L/D_1 = 3$

The RMS amplitude ratio of energy harvester with a symmetric triangular, cylindrical and square prisms downstream tip body as a function of reduced velocity for $L/D_1 = 4$ is presented in Fig. 8. The similar pattern of RMS ratio response was found only for square prism tip body while the others have changed. However, the RMS amplitude still increased with the increasing flow velocity except for square prism tip body. The highest RMS amplitude ratio was found to be 0.89 for triangular tip body at approximately 50 of reduced velocity (Re=20077).

For the symmetric triangular tip body, increasing the L/D_1 ratio from 3 to 4, the reduced velocities with which the energy harvester started to vibrate decreased from 25 to 15. The RMS amplitude ratio continued to rise rapidly until a reduced velocity of approximately 40. The RMS amplitude ratio then gradually rose, which might be explained by the length of cantilever beam to limit the transverse vibration amplitude. However, The RMS amplitude ratio for L/D_1 ratio = 4 was much higher than it had been with the L/D_1 ratio = 3.

On the contrary, when the L/D_1 ratio was raised from 3 to 4, the RMS amplitude for the cylindrical tip body was reduced. Furthermore, it turned out that a peak related to the resonance of the upstream shedding frequency had disappeared. However, the reduced velocity where the harvester started vibrating was approximately the same as 12 of reduced velocity. With further reduced velocity 12, the RMS amplitude ratio continued to increase steadily. The highest RMS amplitude for the L/D_1 = 4 cylindrical tip body was 0.2 at reduced velocity 50. Meanwhile, the square tip body still did not respond to fluid flow, only a tiny vibration was detected. The RMS amplitude was minuscule when compared to the other shapes of downstream tip body.

The experimental results show that when the L/D_1 ratio was increased from 3 to 4, the range of reduced velocity shifted from 5-32 to 8-50. As a result, the reduced velocity range has raised the strong resonance region. This can explain why a peak amplitude related to strong resonance of an upstream shedding vortex could not be found in $L/D_1 = 4$ but could be found in $L/D_1 = 3$ for the cylindrical tip body.

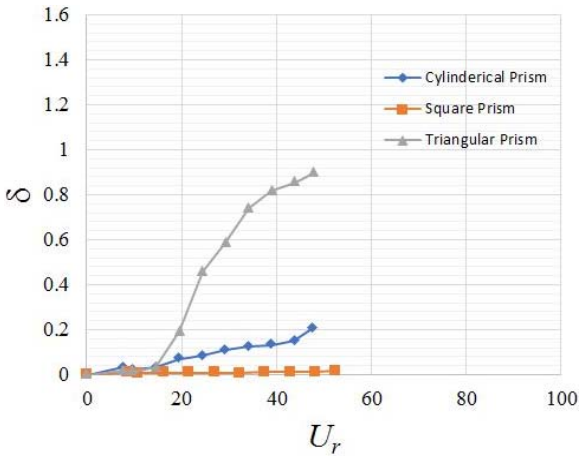

Fig. 8 the RMS amplitude ratio as a function of reduce velocity for $L/D_1 = 4$

Fig. 9 shows the RMS amplitude ratio for $L/D_1 = 5$ for the

energy harvester with a symmetric triangular, cylindrical and square prisms downstream tip body. Increasing the L/D_1 ratio from 4 to 5, the same pattern of RMS ratio response can be found in all shapes of downstream tip body. The RMS amplitude ratio of the triangular and cylindrical tip body still grew with the increase in flow speed. Meanwhile a square tip body barely responded to a rise in flow speed.

The same pattern as L/D_1=4 response can also be found in L/D_1=5 for the triangular tip body. In addition, its RMS amplitude ratio was higher than the RMS amplitude ratio for L/D_1=4 in every Reynolds number. The reduced velocity for vibration to commence declined from 15 to approximately 10. It can be found that increasing the L/D_1 ratio helps to reduce the flow speed and reduced velocity in which the harvester initiates harvester vibration. The highest RMS amplitude ratio for this shape was 1.39 at the maximum flow speed (Re = 20077). Meanwhile, the RMS amplitude for the L/D_1=5 cylindrical tip body was slightly decreased from the RMS amplitude for L/D_1=4. The highest amplitude ratio was only 0.15 compared with that of L/D_1=4 which was 0.21. However, the reduced velocity where the harvester with a cylindrical tip body started vibrating was approximately the same as 12. For the square tip body, there still was little sign of vibration response for L/D_1 = 5. However, if comparing this result with other shapes of tip body, it barely vibrated, even in a strong resonance region. The differences among the L/D_1 ratio for square prism tip body were not distinguishable.

Increasing L/D_1 ratio might result in re-location of separated flow from an upstream bluff body to interact with downstream tip body. The shapes of downstream tip body also had an effect on vortex formation. A cylindrical tip body might allow vortex to form behind it while triangular tip body allow vortex to form on each side of it and square tip body diminish vortex. This can cause different pressure distributions for each shape of downstream tip body. As a result, different characteristic for each configuration was found.

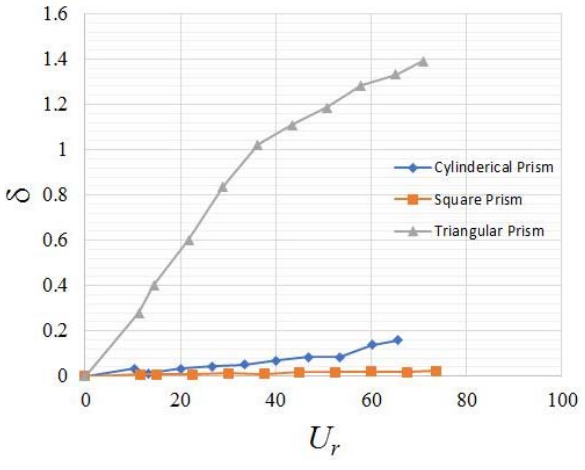

Fig. 9 the RMS amplitude ratio as a function of reduce velocity for L/D_1 = 5

In summary, different configurations of downstream structure were investigated to study their characteristics and search for the proper configurations for energy harvesting applications. The experimental results showed that the RMS amplitude ratio depended on the L/D_1 ratios and shapes of the downstream tip body. The RMS amplitude ratio of the triangular tip body got higher with an increase in L/D_1 ratio. The reduced velocities in which the harvester started vibrating are different for each configuration. The triangular tip body had a lower reduced velocity for vibration to be induced when L/D_1 ratios were raised. Meanwhile the cylindrical tip body obtained a lower RMS amplitude ratio when the L/D_1 ratio was increased. However, it had nearly the same reduced velocity for vibration to start in all L/D_1 ratios. On the contrary, the square tip body did not respond to changes in RMS amplitude ratio in all configurations. The proper configuration for the energy harvester should have a high RMS amplitude ratio and robustness. The harvester with the triangular prism tip body was found to possess such conditions with the highest RMS amplitude ratio of 1.39 and started to vibrate at a lower Reynolds number compared to the others.

B. Frequency Response

According to experimental results, the energy harvester vibrated with almost the same frequency for each L/D_1 ratio. The average of vibration frequency is shown in Table II. Their vibration frequencies were approximately similar to their downstream structure's frequency for each L/D_1 ratio (see Table I).

TABLE II
MEAN FREQUENCY RESPONSE FOR EACH CONFIGURATION

Shape of tip body	L/D_1	Mean structure's vibration frequency, $f_{o\,avg}$ (Hz)
Symmetrical	3	9.3491
Triangular	4	6.4130
Prism	5	4.3163
Cylindrical	3	8.8816
Prism	4	6.4350
	5	4.6694
Square	3	8.5586
Prism	4	5.8432
	5	4.1648

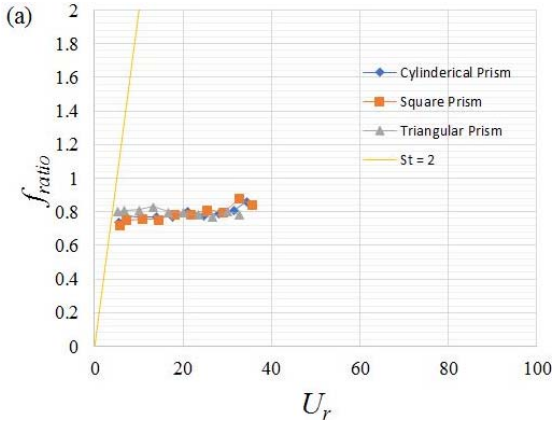

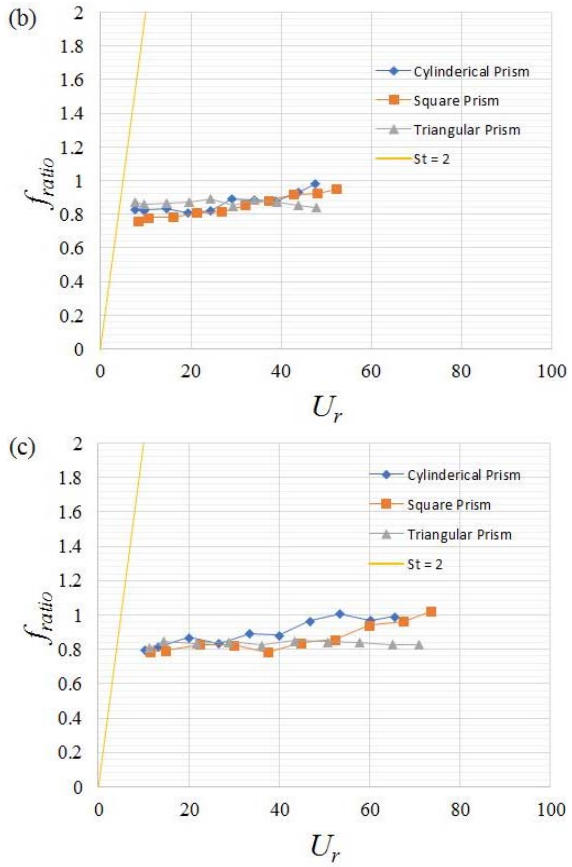

Fig. 10 Frequency response ratio for each configuration (a) $L/D_1 = 3$ (b) $L/D_1 = 4$ (c) $L/D_1 = 5$

The frequency response ratios between the energy harvester's vibration frequency and the energy harvester's natural frequency for each configuration are presented in Fig. 10. All configurations appear to have the same pattern of frequency ratio but a different range of reduced velocity. It can be seen that at a reduced velocity between 4 and 7 where there are the strong resonance of upstream shedding vortex region. The Harvesters with L/D_1 ratios 3 have a frequency ratio close to $St = 2$ line which corresponded to a single cylinder undergo resonance of vortex shedding. Increasing flow velocity further that region, the frequency ratio depart from $St = 2$ line for all L/D_1 ratios but the frequency ratio remained nearly identical, even when the flow velocity was increased for all shapes of downstream tip body.

It can be seen that the harvester vibrated approximately at a natural frequency of each L/D_1 ratio, leading to the suggestion that the harvester operated as a self-excited vibration system [13]. Although all configurations displayed similar patterns of frequency ratio response, their RMS amplitude ratios differed.

C. Electrical and Power Output Response

The influence of load resistance on the electrical energy was investigated. The power generated from the optimal energy harvester as a function of load resistance for each Reynolds number is presented in Fig. 11. Overall, the power output rose with the increase in flow speed which had the same influence as the flow velocity did with the RMS amplitude ratio. However, increasing the load resistance did not always lead to a higher electrical power output. At load resistances between 1 MΩ and 3 MΩ, the power output was reduced sharply due to the fact that the load resistance increased dramatically compared to the voltage output which showed an insignificant increase. Upon increasing the load resistance further in this region, the power output started to increase dramatically and hit a peak at a load resistance between 10 MΩ and 30 MΩ. Then, the power output gradually fell. The maximum power output was found to be 3.19 μW at 20077 Reynolds number at a load resistance of 27 MΩ.

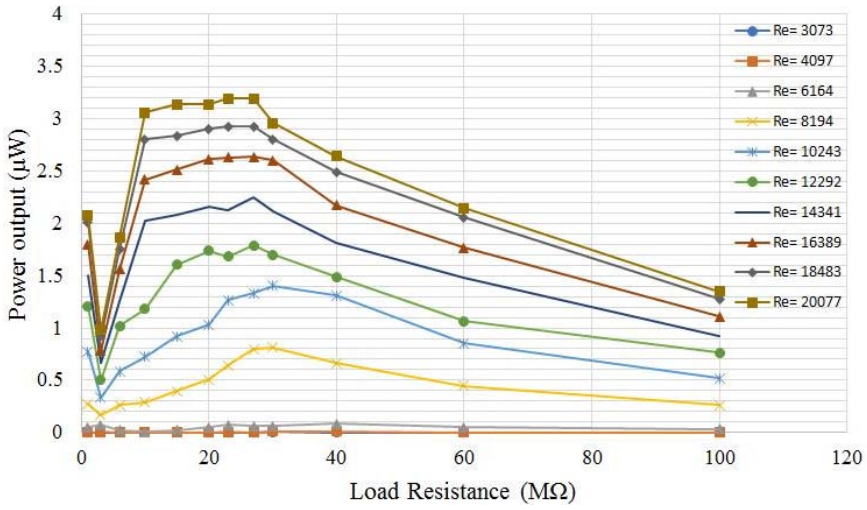

Fig. 11 power output for energy harvester with a symmetric triangular prism tip body and $L/D_1 = 5$ for each load resistance

Table III presented calculated optimal load resistance using (9). The calculated optimal load resistances were found in the range of 26-27 MΩ. This suggest that these calculated load resistance were in accordance with the obtained experimental power output result for all Reynolds Number, except for the range between 3000 and 6200 where there was a tiny response voltage output.

TABLE III
CALCULATED OPTIMAL LOAD RESISTANCE

Flow rate (m/s)	Reynolds Number	Optimal load resistance, (MΩ)
1.5	3073	27.536
2	4097	26.355
3	6146	26.713
4	8194	26.440
5	10243	27.044
6	12292	26.233
7	14341	26.474
8	16389	26.569
9	18438	26.953
10	20077	26.932

Based on the experimental results, increasing flow speed resulted in a rise of power output. Meanwhile the load resistance had a specific value which provides the highest electrical power output. Equation (9) can be confirmed to calculate such an optimal load resistance for piezoelectric type energy harvester according to experimental results.

IV. CONCLUSION

The energy harvesters exploring flow-induce vibration via a piezoelectric beam were designed and tested in a wind tunnel. The experimental results show that the characteristics of energy harvester depend on the shape of downs stream tip body, length of the aluminium cantilever beam and the flow speed. Take for example, the harvester with symmetric triangular prism tip body, which had a tendency to increase in amplitude response with a rise of L/D_1 ratio, while the square prism tip body did not has any response when L/D_1 ratios was increase and the cylindrical tip body vibration amplitude decreased when L/D_1 ratio was increased. However, all configurations turned out to have the similar pattern of frequency ratio response which the harvesters vibrated with frequency close to their structure natural frequency.

The optimization study was performed in order to seek a proper configuration in which has a high vibration amplitude response and robustness. The harvester with symmetric triangular prism tip body had those abilities which it can provide the highest RMS amplitude ratio and start to vibrate at low Reynold number compare to others. This configuration then was tested to generate electrical power output via a piezoelectric beam. The power output of this energy harvester ranged from 0.003 to 3 μW. Its advantage of simplifying and low cost deserves the further study and development.

ACKNOWLEDGMENT

This research was financially supported by the Faculty of Engineering, Kasetsart University, Bangkok, Thailand with an assistant research scholarship for a master degree.

REFERENCES

[1] B. C. Norman, "Power Options for Wireless Sensor Networks," Proc. Proceedings 40th Annual 2006 International Carnahan Conference on Security Technology, 2006,.pp. 17-20.
[2] A. Abdelkefi, A. Alothman, and M. R. Hajj, "Performance analysis and validation of thermoelectric energy harvesters," Smart Materials and Structures, vol. 22, no. 9, p. 095014, 2013.
[3] I. L.Cassidy, J. T. Scruggs, and S. Behrens, "Design of electromagnetic energy harvesters for large-scale structural vibration applications," Proc. SPIE Smart Structures and Materials + Nondestructive Evaluation and Health Monitoring, SPIE, 2011, p. 11.
[4] M. Bryant, and E. Garcia, "Modeling and testing of a novel aeroelastic flutter energy harvester," Journal of Vibration and Acoustics, vol. 133, no. 1, pp. 011010-011010-011011, 2011.
[5] L. A. Weinstein, M. R. Cacan, P. M. So, and P. K. Wright, "Vortex shedding induced energy harvesting from piezoelectric materials in heating, ventilation and air conditioning flows," Smart Materials and Structures, vol. 21 no. 4, p. 045003, 2012.
[6] J. M. McCarthy, A. Deivasigamani, S. J. John, S. Watkins, F Coman, and P. Petersen, "Downstream flow structures of a fluttering piezoelectric energy harvester," Experimental Thermal and Fluid Science, vol. 51, pp. 279-290, 2013.
[7] J. J. Allen, and A. J. Smits, "Energy Harvesting Eel," Journal of Fluids and Structures, vol. 15, no. 3, pp. 629-640, 2001.
[8] S. Mittal, and V. Kumar, "Vortex induced vibrations of a pair of cylinders at Reynolds number 1000," International Journal of Computational Fluid Dynamics, vol. 18, no. 7, pp. 601-614, 2004.
[9] J. Mizushima, and N. Suehiro, "Instability and transition of flow past two tandem circular cylinders," Physics of Fluids, vol. 17, no. 10, p. 104107, 2005.
[10] W. B. Hobbs, and D. L. Hu, "Tree-inspired piezoelectric energy harvesting," Journal of Fluids and Structures, vol. 28, pp. 103-114, 2012
[11] A. Abdelkefi, J. M. Scanlon, E. McDowell, and M. R. Hajj, "Performance enhancement of piezoelectric energy harvesters from wake galloping," Applied Physics Letters, vol. 103, no. 3, p. 033903, 2013.
[12] D. Guyomar, A. Badel, E. Lefeuvre, and C. Richard, "Toward energy harvesting using active materials and conversion improvement by nonlinear processing," IEEE Transactions on Ultrasonics, Ferroelectrics, and Frequency Control, vol. 52, no. 4, pp. 584-595, 2005.
[13] E. Naudascher, and D. Rockwell, "Oscillator-Model Approach To Theidentification And Assessment Offlow-Induced Vibrations In A System," Journal of Hydraulic Research, vol. 18 no. 1, pp. 59-82, 1980.